Jupiter's Equatorial X-ray Emissions Over Two Solar Cycles

A. D. Wibisono[1,2,3]⋆, G. Branduardi-Raymont[1,2], A. J. Coates[1,2], W. R. Dunn[1,2,4] and R. J. French[5]

[1]*Mullard Space Science Laboratory, Department of Space & Climate Physics, University College London, Holmbury St. Mary, Dorking, Surrey, RH5 6NT, UK*
[2]*The Centre for Planetary Science at UCL/Birkbeck, Gower Street, London, WC1E 6BT, UK*
[3]*Royal Observatory Greenwich, London, SE10 8XJ, UK*
[4]*Department of Physics and Astronomy, University College London, Gower Street, London, WC1E 6BT, UK*
[5]*National Solar Observatory, 3665 Innovation Drive, Boulder CO 80303, USA*

ABSTRACT

Jupiter's disk is bright in X-rays as H_2 molecules in the atmosphere are very effective at scattering solar X-rays. K-shell fluorescence from carbon atoms in atmospheric methane is thought to also provide a minor contribution. XMM-Newton has now observed Jupiter over a span of nearly two solar cycles from 2003 to 2021, offering the opportunity to determine whether Jupiter's disk emissions are driven by solar activity or not. We compare the count rates of X-rays of energies 0.2-10.0 keV, 0.2-2.0 keV, 2.1-5.0 keV, and 5.1-10.0 keV from the planet's equatorial region, with the sunspot number and $F_{10.7}$ adjusted solar radio flux. The respective Pearson's Correlation Coefficients for both are 0.88/0.84, 0.86/0.83, 0.40/0.34 and 0.29/0.22 for each energy demonstrating that the low energy X-ray disk emissions are indeed controlled by the Sun's activity. This relationship is less clear for the higher energy emissions, raising questions around the source of these emissions.

Key words: planets and satellites: atmospheres – Sun: X-rays, gamma-rays – planets and satellites: gaseous planets – X-rays: general

1 INTRODUCTION

1.1 Jupiter's X-ray Emissions

X-ray aurorae from Jupiter were first detected in 1979 using instruments onboard the Einstein X-ray Observatory (Metzger et al. (1983)). Data from newer generations of X-ray observatories revealed that these emissions were due to ion charge exchange (e.g. Waite et al. (1994); Cravens et al. (1995, 2003); Branduardi-Raymont et al. (2007b, 2008); Kharchenko et al. (2008); Ozak et al. (2010, 2013); Houston et al. (2018, 2020); Dunn et al. (2020); Wibisono et al. (2021)) and bremsstrahlung radiation (e.g. Branduardi-Raymont et al. (2007b, 2008); Wibisono et al. (2021); Mori et al. (2022).)

Jupiter's disk shines in X-rays and this is most prominent at low and mid latitudes near the equator. The Röntgen Satellite (ROSAT) detected "well-defined emissions emanating from near Jupiter's equator" (Waite et al. (1997)) that were brightest in areas where the reflected sunlight would also be expected to be brightest (Gladstone et al. (1998); Maurellis et al. (2000); Bhardwaj et al. (2005); Branduardi-Raymont et al. (2007b)). It was also found that these emissions were mostly located in regions where the surface magnetic field is weak, which led to the suggestion that they could be due to energetic sulfur and oxygen ions precipitating from the planet's inner radiation belt (Waite et al. (1997); Bhardwaj et al. (2006); McEntee et al. (2022)). However, Gladstone et al. (1998) provided evidence that Jupiter's disk X-ray emissions could be correlated with the Sun's output, as the planet was less X-ray bright between 1994 and 1996, which coincided with a decline in the Sun's $F_{10.7}$ index

of radio flux. Modelling by Maurellis et al. (2000) showed that the Jovian disk emissions are predominantly driven by solar X-ray photons scattering off atmospheric H_2 molecules and it is expected that a small contribution would come from K-shell fluorescence from carbon atoms embedded in methane molecules. Furthermore, their model gave results that agreed with observations by ROSAT in that the planetary disk is brightest in X-rays at the subsolar point.

Contrary to the ROSAT observations, results from the Chandra X-ray Observatory showed that the equatorial emission was uniform (Gladstone et al. (2002); Elsner et al. (2005)) but that the relationship between surface magnetic field strength and the X-ray count rate from low latitudes is more complicated than previously thought (Bhardwaj et al. (2006)). The equator also has a harder spectrum than that from the aurorae and is best fitted using a model that simulates the emission lines from a solar coronal plasma (the MEKAL model) with the addition of gaussian lines at 1.35 keV and 1.86 keV which correspond to Mg XI and Si XIII ions, respectively (Branduardi-Raymont et al. (2004, 2007a)). The APEC (Astrophysical Plasma Emission Code) model is now typically used to fit Jupiter's disk emission (e.g. Dunn et al. (2020)). Emissions from Mg XI and Si XIII ions are tell tale signs of a flaring Sun (Branduardi-Raymont et al. (2007a); Bhardwaj et al. (2006)).

Observational results from XMM-Newton and Chandra also strengthen the evidence for the case of solar scattering. Firstly, the Jovian low latitude X-rays increased in intensity during periods of high solar activity, such as that of the 2003 Halloween Storm. Moreover, the day to day variabilities in the lightcurves from Jupiter's equator and the solar X-rays match (Branduardi-Raymont et al. (2004); Bhardwaj et al. (2005)). XMM-Newton's observations took place over two of its orbits between 25-29 November 2003. Unfortunately,

⋆ E-mail: affelia.wibisono.18@ucl.ac.uk

the largest solar flare that occurred in this time period happened during XMM-Newton's perigee passage, which meant that its effects on Jupiter's disk emission could not be observed. However, Dunn (2022) and the Supporting Information for Dunn et al. (2016) showed that the equatorial lightcurve peaked with the occurrence of a solar flare and that the aurorae did not respond to the solar flare in the same way. Calculations by Cravens et al. (2006) confirmed that Jupiter's disk X-ray emissions are indeed due to solar scattering. Recently McEntee et al. (2022) undertook a statistical study using data from Chandra to demonstrate that Jupiter's equatorial X-ray emissions are correlated with solar flux, although there also appeared to be slight enhancements in the disk emissions at regions with low surface magnetic field strength of 2-3.5 G.

1.2 The Solar Cycle

The Sun's magnetic activity waxes and wanes roughly every 11 years in what is known as the Schwabe cycle (Vecchio, A. et al. (2017)). This cycle is most easily tracked by observing the number of sunspots on the Sun. Sunspots are regions where the solar magnetic field is particularly strong and this enhanced magnetic activity and high concentration of magnetic field flux prevent convective heat transport from the Sun's interior travelling up to the photosphere, resulting in the spots being darker than the rest of the Sun's disk (Aschwanden (2014); Oyedokun & Cilliers (2018)). It is common for the Sun to have no sunspots at the start of its cycle when its activity is at a minimum, and the number of sunspots on the Sun's photosphere then increases with solar activity. The Sun's magnetic field also governs other phenomena, such as its radio, UV and X-ray emissions, and how frequently flares and coronal mass ejections are released. As a result, these follow the same magnetic cycle as the sunspots (Aschwanden (2014); Hathaway (2010)).

Another long-established method to indicate the level of solar activity is to measure the hourly-averaged solar radio flux at a wavelength of 10.7 cm, also known as the $F_{10.7}$ index. These emissions originate from the Sun's upper chromosphere and lower corona (Tapping (2013)). Three values are given for each $F_{10.7}$ measurement. The first is the observed value which records how much of the emissions, because of the solar activity, reach the Earth. This is why the observed value tends to be used for terrestrial phenomena studies. The adjusted value takes into account the Earth's varying distance from the Sun and this measurement is used for solar studies. The Series D Flux attempts to measure the absolute flux density at the 10.7 cm wavelength. This value is obtained by multiplying the adjusted value by a scaling factor of 0.9, however, recent work suggests that this factor may need to be revised (NRC Space Weather Canada (2021)).

In this work we utilise two solar cycles of XMM-Newton observations of Jupiter to explore the relationship between the solar X-ray emission and different energy regimes of Jupiter's equatorial X-ray emission, as well as the adjusted value of the $F_{10.7}$ index with the X-ray count rates from Jupiter's equator.

1.3 Instrumentation

XMM-Newton's payload consists of three X-ray telescopes and one optical/UV telescope. At the focus of one of the X-ray telescopes is the pn camera of the European Photon Imaging Camera (EPIC) which is primarily used as an imaging spectrometer. The EPIC-pn camera has an effective area of 1227 cm^2 at 1 keV, a spectral resolution of E/ΔE ~ 5 − 50, a timing resolution of 0.03 ms and the full width at half maximum (FWHM) of its point spread function (PSF) is 6.6 ″

at 1.5 keV (Strüder et al. (2001)). EPIC-pn's high sensitivity makes it ideal for Jupiter X-ray studies since in a typical observation EPIC-pn will detect from 0.5 to a few X-ray photons per minute from Jupiter.

The EPIC instrument also comprises two Metal Oxide Semiconductor (MOS) cameras at the foci of the remaining X-ray telescopes. These telescopes are fitted with gratings that allow roughly half of the incoming X-ray flux to fall onto the MOS CCDs. EPIC-MOS has an effective area of 922 cm^2 at 1 keV, a spectral resolution of E/ΔE ~ 10 − 50 and a time resolution of 1.5 ms. At FWHM, MOS1 has a PSF of 6″ while MOS2 has a PSF of 4.5 ″ at 1.5 keV (Jansen et al. (2001)). The three EPIC cameras are sensitive to X-rays with energies 0.1-15 keV and each has circular field of view with a 30′ diameter (Turner et al. (2001)).

2 EQUATORIAL COUNT RATES FROM EPIC

As of December 2022, XMM-Newton has observed Jupiter for a total duration of more than 2 Ms over 25 different campaigns since 2003. However, a few have processing issues and consequently we chose to leave them out of this analysis rather than introduce potential anomalies. This leaves 19 observations with EPIC data that can be analysed and compared. These observations are listed in Table 1 and overlaid over a plot of the monthly average sunspot number in Figure 1. Although the observations from November 2003 were technically during the descending phase of Cycle 23, they have been classified here as occurring at solar maximum because the Sun had comparable number of sunspots during those observations as the one at the peak of Cycle 24 in 2014.

The data in this study were treated in the same way as described in Branduardi-Raymont et al. (2007b) and Wibisono et al. (2020) and analysed using the XMM-Newton Science Analysis Software (SAS) v. 19.1.0 released on 17 March 2021. EPIC-pn images of Jupiter from the 19 observations used in this study are shown in Figure 2.

Jupiter's angular diameter, north pole tilt angle and center of the planet for each observation were obtained from the NASA JPL Horizons System app (https://ssd.jpl.nasa.gov/horizons/app.html#/). These were used to determine the planet's disk extension in the SAOImage DS9 astronomical imaging and data visualization application. The northern and southern aurorae were located by eye with ovals while Jupiter's equatorial region was isolated with a rectangular region. This rectangular region had a height of 20% of Jupiter's angular diameter and a width that did not go beyond the planet's disk. Each image was checked to ensure that the rectangular equatorial region did not include parts of the aurorae to avoid contamination. The aurorae and equatorial regions for each observation are shown in Figure 2 and the Supporting Information (Figure A1) shows the image from 25 Nov 2003 with Jupiter's disk marked on also.

It stands to reason that since the disk X-ray emissions from Jupiter are mostly caused by elastic scattering of solar X-rays, that the two would correlate. Previous studies have compared the equatorial X-ray emissions from Jupiter with that of the Sun using measurements by TIMED/SEE and GOES data, however, they have only done so for a small number of observations separated by a few days (e.g. Bhardwaj et al. (2005, 2006); Branduardi-Raymont et al. (2007a)). Dunn et al. (2020) compared the fluxes for Jupiter's equatorial X-rays over one solar cycle using XMM-Newton and Chandra data. These observations took place in February-March 2007, October 2011, April 2014 and May 2016. While the results indeed show that Jupiter's equatorial X-rays vary with the solar cycle (the fluxes were 0.21 GW and 0.76 GW at solar minimum and maximum, respectively), they were
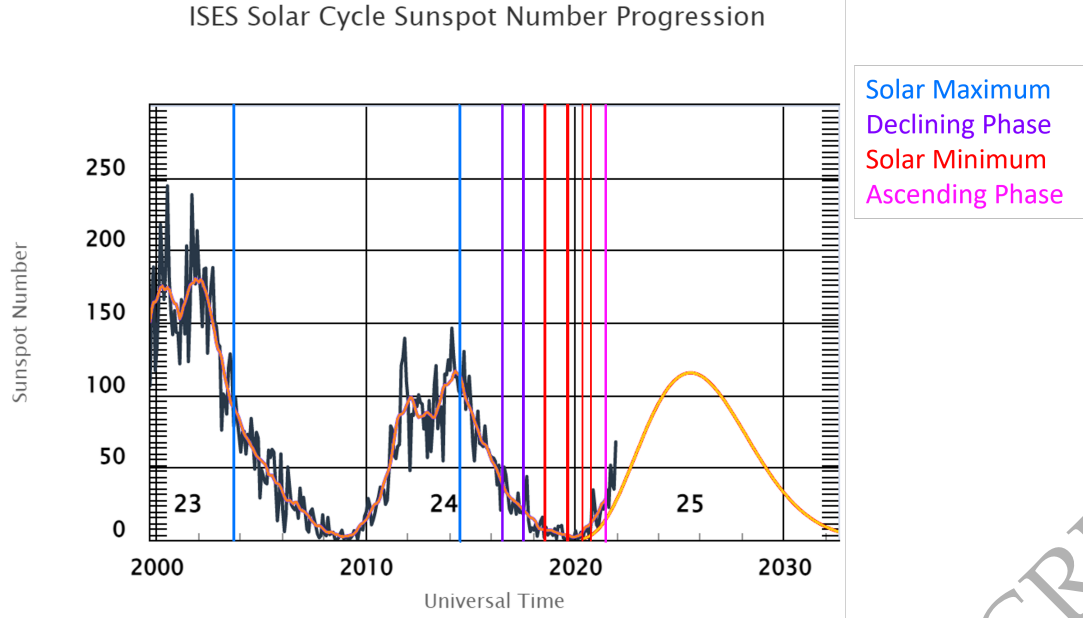
Figure 1. Times of the XMM-Newton observations (vertical lines) analysed in this study overlaid over a plot of the monthly average sunspot number (sunspot number from https://www.sidc.be/silso/datafiles). The blue lines indicate observations taken at or around high solar activity, purple show those taken during the declining phase of the solar cycle, red lines are for observations taken at solar minimum and pink highlight those taken during the ascending phase. Note that the number of lines do not match the number of observations because some of the observations were taken within the same month and apparently thicker lines are two lines marking two observations that happened closely in time.

Table 1. The 19 XMM-Newton observations used in this study. The S-J and J-E distance columns show the median distance between the Sun and Jupiter, and between Jupiter and the Earth, respectively, during the observation. Jupiter's angular diameter is also the median angular diameter during the observation. The counts from the northern aurora (N), southern aurora (S) and equatorial region (Eq) are the total counts from EPIC-pn and EPIC-MOS for the entire observation. These X-ray photons have energies 0.2-10.0 keV.

Observation date	Duration (ks)	Solar cycle phase	S-J distance (AU)	J-E distance (AU)	J angular diameter ($''$)	N counts	S counts	Eq counts	Total counts
25/11/2003	122	Max	5.40	5.53	35.65	3521	2259	928	6708
27/11/2003	117	Max	5.40	5.49	35.90	2333	1672	1721	5726
15/04/2014	41	Max	5.23	5.37	36.74	1308	1215	780	3303
20/04/2014	43	Max	5.23	5.43	36.29	1169	820	476	2465
18/05/2016	50	Dec	5.44	4.94	39.91	1189	530	247	1966
24/05/2016	44	Dec	5.44	5.18	38.08	885	371	176	14325
19/06/2017	84	Dec	5.45	5.10	38.65	830	515	256	1601
10/07/2017	137	Dec	5.45	5.44	36.22	2870	924	505	4299
16/07/2017	94	Dec	5.45	5.53	35.65	1817	959	252	3028
16/07/2018	45	Min	5.39	4.98	39.69	612	433	118	1163
27/08/2018	37	Min	5.38	5.61	35.15	939	817	138	1894
08/09/2019	128	Min	5.27	5.18	38.04	2271	1682	374	4327
10/09/2019	120	Min	5.27	5.21	37.81	1804	914	184	2903
12/09/2019	129	Min	5.27	5.24	37.60	2557	1440	234	4231
08/04/2020	134	Min	5.19	5.18	39.02	2005	1217	357	3579
31/10/2020	111	Min	5.12	5.34	36.91	1636	811	544	2991
10/05/2021	113	Asc	5.05	5.10	39.62	2620	1041	529	4190
02/06/2021	76	Asc	5.05	4.76	41.45	2373	843	488	3704
07/06/2021	117	Asc	5.05	4.67	42.22	2628	1114	940	4682

simply case-studies and did not track how Jupiter's disk responds to the Sun's varying activity over its cycle. A long-term statistical study comparing Jupiter's X-ray emissions from its equatorial region and the solar X-ray flux using Chandra data has also recently been completed (McEntee et al. (2022)). Here we compared the monthly average sunspot number and the adjusted $F_{10.7}$ value with the EPIC-pn and EPIC-MOS X-ray photon count rates from Jupiter's equatorial region for each of the 19 XMM-Newton observations. These count

rates were normalised for the distance between Jupiter and Earth so the observations could be compared with each other. This was done over several energy ranges to explore energy dependence (Figure 3). Although the distance between the Sun and Jupiter does vary between observations, as shown in Table 1, the Jupiter-Earth distance can differ by a greater distance and can range between 4.20-6.20 AU. However, XMM-Newton cannot observe Jupiter when it is at opposition and so the distance between the spacecraft and Jupiter will
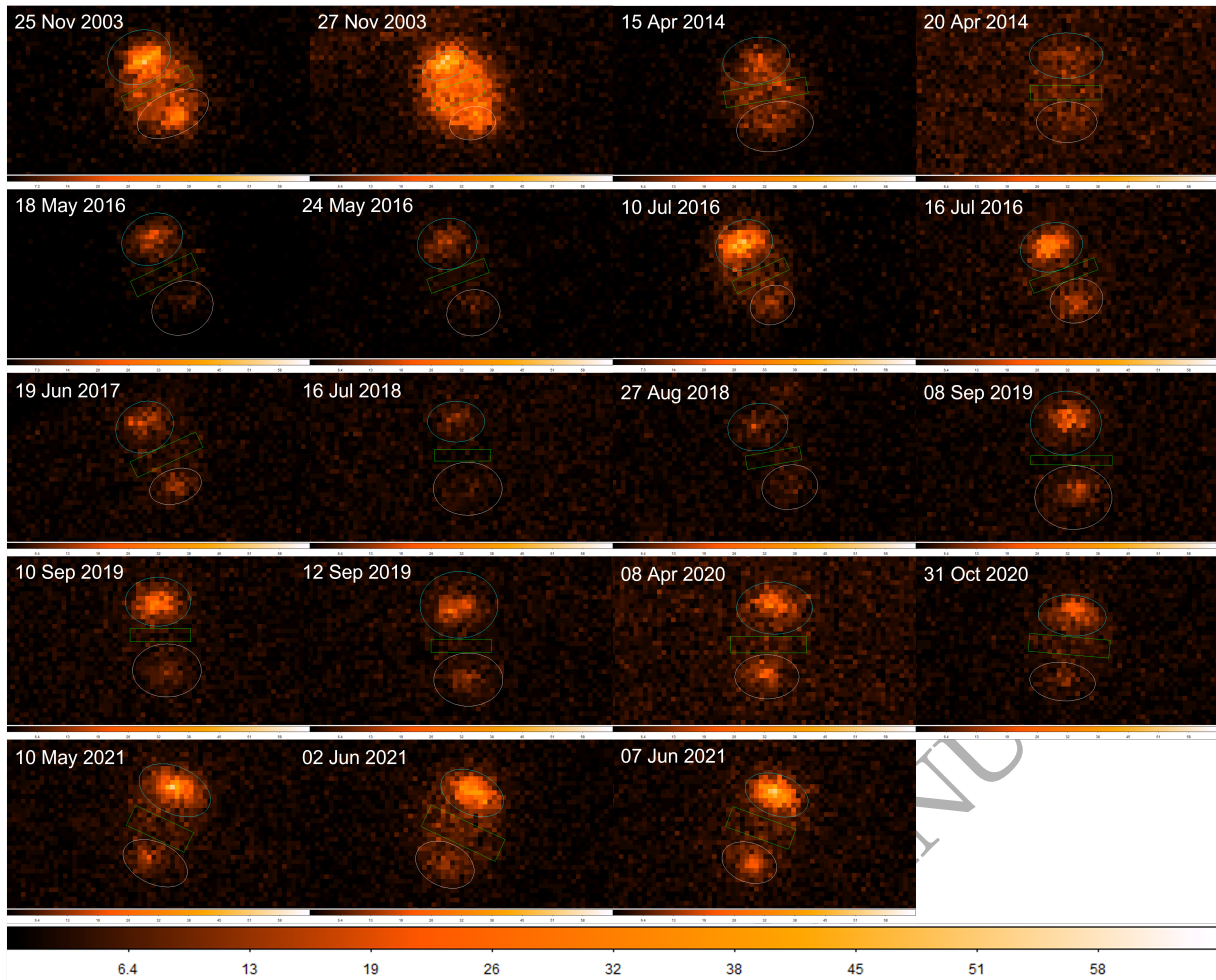
Figure 2. XMM-Newton EPIC-pn images of Jupiter from all 19 observations. Note how the planet's equatorial emissions and orientation vary over time. The 0.2-2.0 keV equatorial emissions are controlled by the Sun's activity over its cycle and the orientation of the planet with respect to XMM-Newton changes over Jupiter's orbit around the Sun. The X-ray photons were re-registered onto Jupiter's disk giving the appearance that the planet is static on the CCD while background sources become streaks (see Figure 1 from Dunn et al. (2021)). The northern lights are circled in blue, the equatorial regions are shown by the green boxes, and the southern lights are marked by the white ovals. The colour bar for each image shows the number of X-ray photons on each pixel with the brightest pixel having a maximum of 64 photons.

always be larger than this minimum distance. Thus why we chose to normalise the count rates for the Jupiter-Earth distance.

Panel A in Figure 3 illustrates that there is a very strong correlation between the sunspot number and the scattered equatorial X-rays over all the energies measured by EPIC. This correlation is also present when only the low energy (0.2-2.0 keV) band is considered as shown by panel B. However, this relationship is not so strong for X-rays with energies above 2.0 keV as shown by panels C and D where only the point for 20 April 2014 is consistent with the solar maximum. The count rate for this observation remained high but this could be due to the fact that this particular dataset was particularly noisy with a high background and short exposure time. Panels E-H show similar plots that compare the adjusted value for the 10.7 cm solar flux with Jupiter's equatorial X-ray count rates. The same positive correlation from panels A and B are shown in panels E and F, but this relationship is not as clear in panels G and H. Table 2 lists the count rates shown in Figure 3.

A Pearson's test was applied for each energy band to ensure that the connection between Jupiter's equatorial X-rays and the solar cycle was statistically significant. Figure 3 has the results from these tests,

showing strong positive correlation only in the 0.2-2.0 keV and full energy ranges for both indicators of solar activity.

3 DISCUSSION

XMM-Newton has acquired measurements of Jupiter's X-ray emissions since 2003. The sources of these emissions are at the planet's poles due to ion charge exchange and bremsstrahlung radiation, and in the disk where they arise from elastic scattering and fluorescence of solar X-ray photons. With a collection of datasets that span almost 20 years, Jupiter's disk emissions can be evaluated with respect to the solar cycle.

This study used data from the XMM-Newton's EPIC-pn and EPIC-MOS cameras to demonstrate that the X-rays from Jupiter's low latitude region are indeed driven by the Sun's activity as shown by panel A in Figure 3. This relationship is strong for the equatorial soft X-ray emissions but is much weaker for energies above 2.0 keV.

Peres et al. (2000) modelled the X-ray spectra of the Sun at solar maximum with and without flares, and at solar minimum as if they were taken by an astrophysical X-ray observatory such as ROSAT
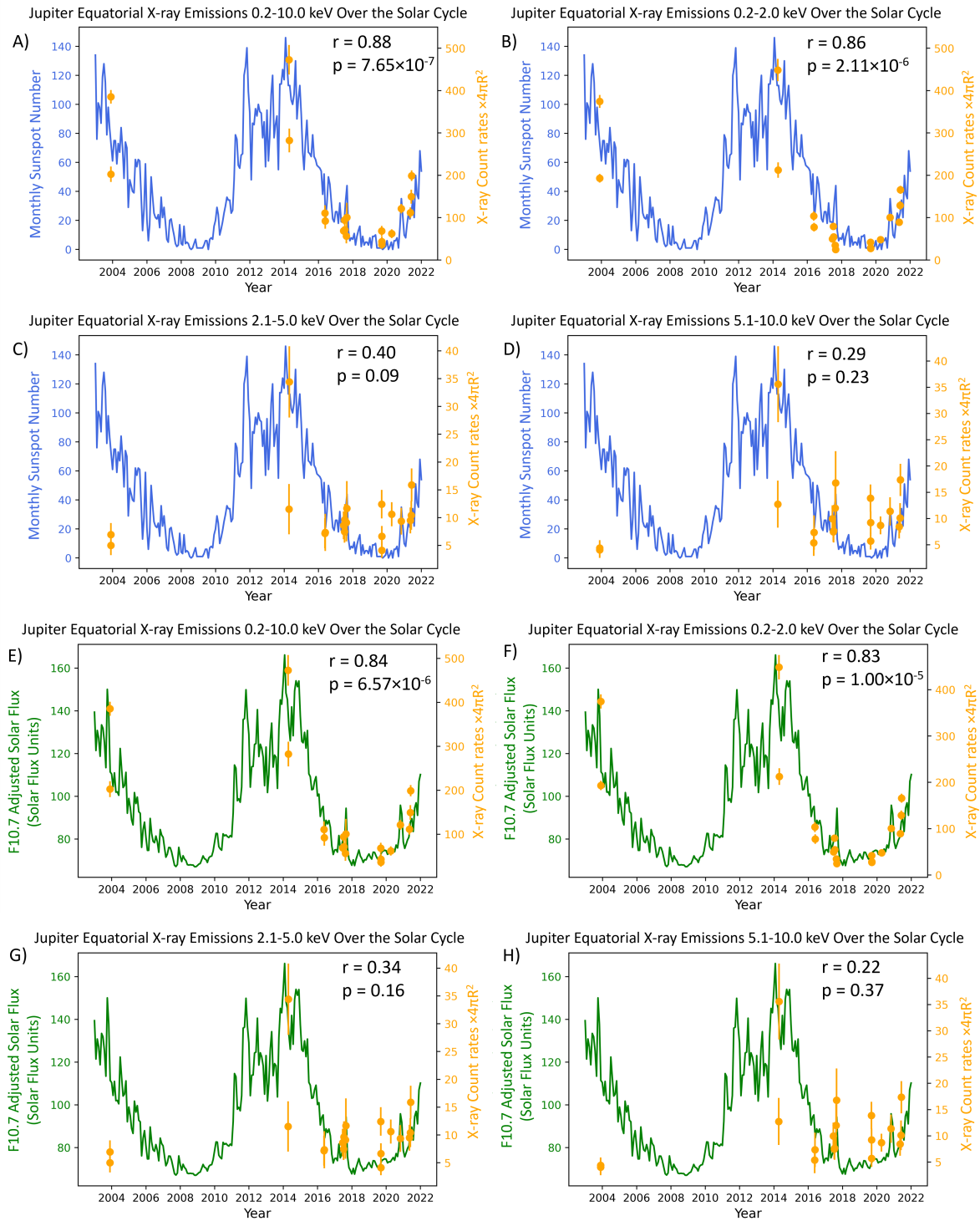
Figure 3. The average monthly sunspot number (blue), the adjusted $F_{10.7}$ solar radio flux (green) and the X-ray count rates observed from Jupiter's equator (orange) over time. Panels A and E plot the X-rays with energies of 0.2-10.0 keV, panels B and F for those 0.2-2.0 keV, panels C and G for those between 2.1-5.0 keV and panels D and H show the X-rays with energies 5.1-10.0 keV as measured by EPIC. Data for the $F_{10.7}$ adjusted solar flux were taken from https://lasp.colorado.edu/lisird/data/noaa_radio_flux/. The count rates for each observation have been corrected for the Jupiter-Earth distance (R in Astronomical Units). The correlation coefficient (r) and p-values (p) for each energy range are shown on the respective panels.

Table 2. Count rates of X-ray photons observed from Jupiter's equatorial region for all 19 observations and energy ranges. The units are $\times 4\pi$ s^{-1}. The dates show the start of the observations. We have accounted for the different distances between Jupiter and XMM-Newton (i.e. the Earth) for each observation. The graphs for this table are found in Figure 3.

Observation date	0.2-10.0 keV	0.2-2.0 keV	2.1-5.0 keV	5.1-10.0 keV
25/11/2003	202.58 ± 18.18	193.19 ± 10.17	5.02 ± 1.76	4.37 ± 1.50
27/11/2003	385.43 ± 16.0	374.46 ± 15.33	6.94 ± 2.08	4.03 ± 1.54
15/04/2014	472.75 ± 34.97	448.51 ± 26.42	11.52 ± 4.52	12.73 ± 4.48
20/04/2014	282.36 ± 28.07	212.37 ± 18.05	34.41 ± 6.42	35.59 ± 7.23
18/05/2016	110.85 ± 18.60	103.67 ± 10.96	7.18 ± 2.70	5.39 ± 2.50
24/05/2016	92.28 ± 18.37	77.60 ± 10.29	7.34 ± 3.34	7.34 ± 3.27
19/06/2017	68.90 ± 10.34	49.79 ± 5.87	8.61 ± 2.49	9.96 ± 2.55
10/07/2017	94.40 ± 10.68	79.45 ± 6.20	7.48 ± 1.98	7.48 ± 1.91
16/07/2017	71.40 ± 15.27	54.68 ± 6.37	9.63 ± 2.81	7.65 ± 2.22
16/07/2018	56.52 ± 17.10	34.49 ± 6.39	9.10 ± 3.36	11.98 ± 4.05
27/08/2018	100.65 ± 34.40	24.80 ± 6.94	11.67 ± 4.91	16.78 ± 6.05
08/09/2019	68.30 ± 12.29	42.00 ± 4.44	12.42 ± 2.56	13.88 ± 2.60
10/09/2019	36.42 ± 10.29	28.74 ± 3.77	4.13 ± 1.38	5.71 ± 1.62
12/09/2019	43.19 ± 12.23	27.32 ± 3.66	6.65 ± 1.86	9.23 ± 2.15
08/04/2020	62.11 ± 10.53	48.02 ± 4.62	10.61 ± 2.16	8.70 ± 1.69
31/10/2020	121.19 ± 11.24	100.47 ± 7.67	9.36 ± 2.41	11.36 ± 2.69
10/05/2021	111.66 ± 12.67	89.28 ± 6.91	9.50 ± 2.34	8.44 ± 2.25
02/06/2021	149.54 ± 16.54	129.01 ± 10.24	10.42 ± 2.61	10.11 ± 2.83
07/06/2021	199.02 ± 12.68	165.78 ± 9.56	15.88 ± 2.96	17.36 ± 3.07

or the Advanced Satellite for Cosmology and Astrophysics (ASCA). They show that the solar X-ray spectrum cuts off just above 2.0 keV at solar maximum and at ~1.5 keV at solar minimum (Figure 7 in Peres et al. (2000)). On the other hand, the Sun does emit X-rays with higher energies during flares as shown in their Figure 8. This may explain why the correlation found in Figure 3 is strong when X-rays below 2.0 keV are taken into account and why the relationship between the X-ray count rates and sunspot number is weaker for the higher energy range since the Sun rarely emits X-rays with these energies.

We discuss four possible suggestions to explain the presence of >2.0 keV X-rays, particularly for the peak at 20 April 2014. Firstly, it could be due to an instrumental effect. The EPIC-pn experienced flaring events over 45% of its exposure time during this observation. The background count rate for the full energy range at this time was also an order of magnitude higher than for the rest of the observations (0.11 counts s^{-1} compared to 0.01-0.08 counts s^{-1}). Solar flares can also emit high energy X-rays that are then scattered by Jupiter. The solar X-ray flux from GOES shows that there were no large Earth-directed flares from the Sun in the hours before and during this observation (see Figure B1 in the Supporting Information). It is possible that one such flare was not visible at Earth orbit, but was incident at Jupiter since the Jupiter-Sun-Earth angle was ~83°at the time of the observation. Alternatively, if the X-ray disk emissions are due to precipitating sulfur and oxygen from the radiation belts then it would be expected that they would have energies below 1.0 keV. While there are some known sulfur lines above 2.0 keV, we consider it unlikely that the high energy X-rays from Jupiter's equator would be present without their low energy counterpart from the forest of sulfur lines between 0.2 and 0.5 keV. At Earth, electrons from the radiation belts can precipitate and emit X-rays through bremsstrahlung (e.g. Berger & Seltzer (1972); Stadsnes et al. (1997)). The same could be the case for Jupiter. Finally, some of the disk emissions above 2.0 keV could be contamination from the aurorae. For the second observation in April 2014, the high background seems the most likely solution, however, future work could explore the expected bremsstrahlung signatures from electron radiation belt precipitation (e.g. Dunn et al. (2022)).

4 CONCLUSION

Studying the X-ray emissions from Jupiter's equator reveals that at low energies, they vary with the solar cycle and are driven by the Sun's activity, in agreement with the literature. However, this correlation weakens above 2.0 keV as the planet tends to release a small flux of high energy X-rays even at solar maximum. Future work may be needed to explore the possibility of distinguishing components that are related to radiation belt electron precipitation from the high energy background.

DATA AVAILABILITY

All of the XMM-Newton dataset featured in this study can be found in https://www.cosmos.esa.int/web/xmm-newton/xsa. The monthly sunspot number used in Figure 1) is from https://www.sidc.be/silso/datafiles). Data for the F10.7 cm adjusted solar flux was taken from https://lasp.colorado.edu/lisird/data/noaa_radio_flux/. The GOES plot from the Supporting Information was obtained from https://www.polarlicht-vorhersage.de/goes-archive. To download the XMM-Newton Science Analysis software, go to this webpage https://www.cosmos.esa.int/web/xmm-newton/download-and-install-sas. The XSPEC spectral fitting package can be downloaded from https://heasarc.gsfc.nasa.gov/xanadu/xspec/.

REFERENCES

Aschwanden M. J., 2014, in Spohn T., Breuer D., Johnson T. V., eds, , Encyclopedia of the Solar System (Third Edition), third edition edn, Elsevier, Boston, pp 235–259, doi:https://doi.org/10.1016/B978-0-12-415845-0.00011-6, https://www.sciencedirect.com/science/article/pii/B9780124158450000116

Berger M., Seltzer S., 1972, Journal of Atmospheric and Terrestrial Physics, 34, 85

Bhardwaj A., et al., 2005, Geophysical Research Letters, 32

Bhardwaj A., Elsner R. F., Gladstone G. R., Waite J. H., Branduardi-Raymont G., Cravens T. E., Ford P. G., 2006, Journal of Geophysical Research: Space Physics, 111

Branduardi-Raymont G., Elsner R., Gladstone G., Ramsay G., Rodriguez P., Soria R., Waite Jr J., 2004, Astronomy & Astrophysics, 424, 331

Branduardi-Raymont G., et al., 2007a, Planetary and Space Science, 55, 1126

Branduardi-Raymont G., et al., 2007b, Astronomy & Astrophysics, 463, 761–774

Branduardi-Raymont G., Elsner R. F., Galand M., Grodent D., Cravens T. E., Ford P., Gladstone G. R., Waite J. H., 2008, Journal of Geophysical Research Space Physics, 113

Cravens T. E., Howell E., Waite Jr J., Gladstone G., 1995, Journal of Geophysical Research Space Physics, 100, 17153

Cravens T. E., Waite J. H., Gombosi T. I., Lugaz N., Gladstone G. R., Mauk B. H., MacDowall R. J., 2003, Journal of Geophysical Research: Space Physics, 108

Cravens T. E., Clark J., Bhardwaj A., Elsner R., Waite Jr. J. H., Maurellis A. N., Gladstone G. R., Branduardi-Raymont G., 2006, Journal of Geophysical Research: Space Physics, 111

Dunn W. R., 2022, X-Ray Emissions from the Jovian System. Springer Nature Singapore, Singapore, pp 1–56, doi:10.1007/978-981-16-4544-0_73-1, https://doi.org/10.1007/978-981-16-4544-0_73-1

Dunn W. R., et al., 2016, Journal of Geophysical Research Space Physics, 121, 2274

Dunn W. R., et al., 2020, Journal of Geophysical Research: Space Physics, n/a, e2019JA027219

Dunn W. R., et al., 2021, Journal of Geophysical Research: Space Physics, 126, e2020JA028739

Dunn W. R., et al., 2022, Geophysical Research Letters, 49, e2021GL097390

Elsner R. F., et al., 2005, Journal of Geophysical Research Space Physics, 110

Gladstone G. R., Waite J. H., Lewis W. S., 1998, Journal of Geophysical Research: Planets, 103, 20083

Gladstone G. R., et al., 2002, Nature, 415, 1000

Hathaway D. H., 2010, Living Reviews in Solar Physics, 7

Houston S. J., Ozak N., Young J., Cravens T. E., Schultz D. R., 2018, Journal of Geophysical Research: Space Physics, 123, 2257

Houston S. J., et al., 2020, Journal of Geophysical Research: Space Physics, 125, e2019JA027007

Jansen F., et al., 2001, A&A, 365, L1

Kharchenko V., Bhardwaj A., Dalgarno A., Schultz D. R., Stancil P. C., 2008, Journal of Geophysical Research: Space Physics, 113

Maurellis A. N., Cravens T. E., Gladstone G. R., Waite J. H., Acton L. W., 2000, Geophysical Research Letters, 27, 1339

McEntee S. C., et al., 2022, Journal of Geophysical Research: Space Physics, 127, e2022JA030971

Metzger A. E., Gilman D. A., Luthey J. L., Hurley K. C., Schnopper H. W., Seward F. D., Sullivan J. D., 1983, Journal of Geophysical Research Space Physics, 88, 7731

Mori K., et al., 2022, Nature Astronomy, 6, 442

NRC Space Weather Canada 2021, About the solar flux data, https://www.spaceweather.gc.ca/forecast-prevision/solar-solaire/solarflux/sx-3-en.php

Oyedokun D. T., Cilliers P. J., 2018, in Zobaa A. F., Abdel Aleem S. H., Abdelaziz A. Y., eds, , Classical and Recent Aspects of Power System Optimization. Academic Press, pp 421–462, doi:https://doi.org/10.1016/B978-0-12-812441-3.00016-1, https://www.sciencedirect.com/science/article/pii/B9780128124413000161

Ozak N., Schultz D. R., Cravens T. E., Kharchenko V., Hui Y.-W., 2010, Journal of Geophysical Research: Space Physics, 115

Ozak N., Cravens T. E., Schultz D. R., 2013, Geophysical Research Letters, 40, 4144

Peres G., Orlando S., Reale F., Rosner R., Hudson H., 2000,] 10.1086/308136, 528, 537

Stadsnes J., Aarsnes K., Bjordal J., 1997, Advances in Space Research, 20, 1043

Strüder L., et al., 2001, A&A, 365, L18

Tapping K. F., 2013, Space Weather, 11, 394

Turner M. J. L., et al., 2001, A&A, 365, L27

Vecchio, A. Lepreti, F. Laurenza, M. Alberti, T. Carbone, V. 2017, A&A, 599, A58

Waite J. H., et al., 1994, Journal of Geophysical Research Space Physics, 99, 14799

Waite J. H., Gladstone G. R., Lewis W. S., Drossart P., Cravens T. E., Maurellis A. N., Mauk B. H., Miller S., 1997, Science, 276, 104

Wibisono A. D., et al., 2020, Journal of Geophysical Research: Space Physics, 125, e2019JA027676

Wibisono A. D., et al., 2021, Monthly Notices of the Royal Astronomical Society

APPENDIX A: DEFINING THE EQUATORIAL REGION

Figure 2 in the main text has the EPIC-pn images of Jupiter for each observation that are marked with the auroral and equatorial regions. The main text also describes how the equatorial regions were defined. The image in Figure A1 is from the observation taken on 25 Nov 2003 which shows more clearly how the equatorial region was determined.

APPENDIX B: GOES SOLAR X-RAY FLUX APRIL 2014

The main text describes that there was a surprisingly high X-ray count rate from Jupiter's equator at energies above 2.0 keV on 20 April 2014. Figure B1 shows that there were no large X-ray flares measured at Earth orbit in the hours before and during this observation. While it is possible that such a flare was incident on Jupiter, we believe that the most likely explanation for the peak X-ray count rate was instrumental rather than physical.
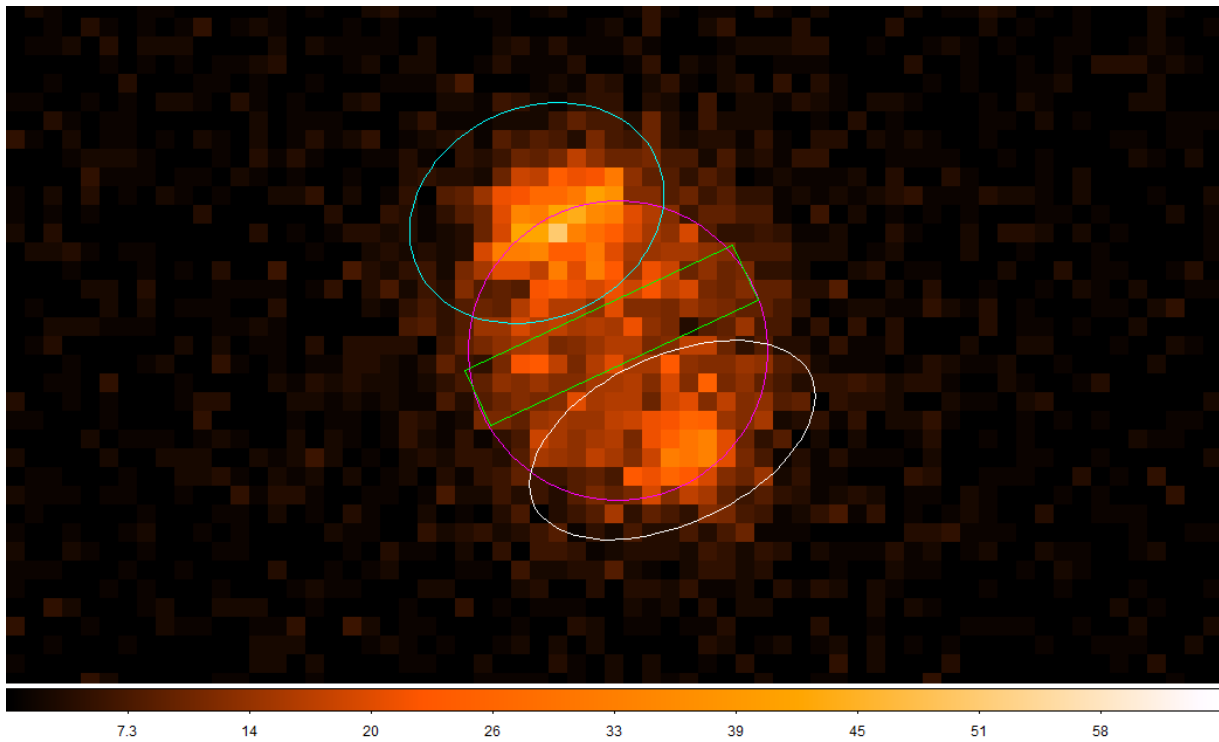
Figure A1. EPIC-pn image of Jupiter. The magenta circle marks the planet's disk, the blue and white ovals are the northern and southern aurorae, respectively, and the green rectangle is the equatorial region.
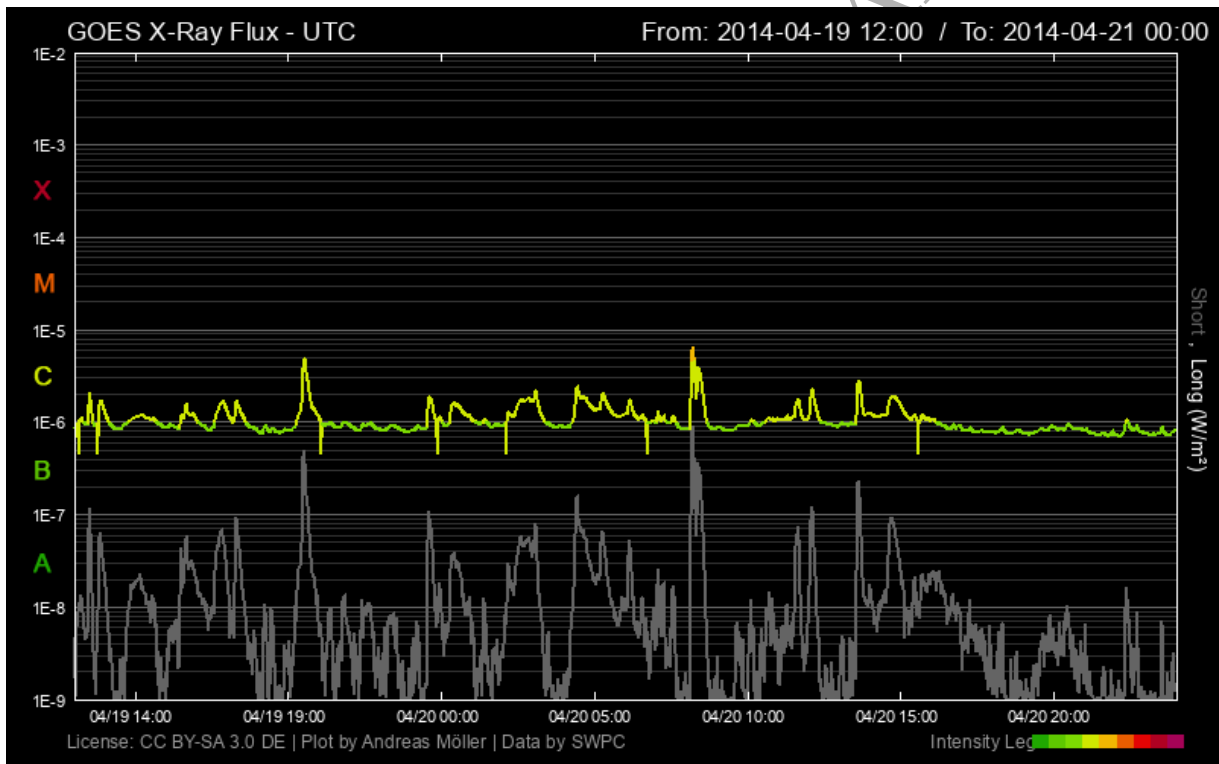
Figure B1. The GOES X-ray flux in the hours before and during the 20 April 2014 XMM observation. The grey plot shows the short-wavelength X-ray band (3.10-24.80 keV) while the colour plot shows that of the long-wavelength X-ray band (1.55-12.40 keV). Plot is produced from https://www.polarlicht-vorhersage.de/goes-archive/.